BUTTERWORTH HEINEMANN

Conjugate natural convection from an array of discrete heat sources: part 2 — a numerical parametric study

T. J. Heindel, F. P. Incropera, and S. Ramadhyani
Heat Transfer Laboratory, School of Mechanical Engineering, Purdue University, West Lafayette, IN, USA

Coupled conduction and natural convection transport within a discretely heated cavity have been investigated numerically. One vertical wall of the cavity is composed of discrete, isoflux heat sources mounted in a substrate of finite thermal conductivity. The opposite vertical wall and the horizontal walls are assumed to be isothermal and adiabatic, respectively. The governing steady-state partial differential equations for the fluid and solid region are solved simultaneously using a control volume formulation, coupled with an additive correction multigrid procedure that increases the convergence rate of the solution. The fluid Prandtl number and heater/fluid thermal conductivity ratio are fixed at 25 and 2350, respectively, corresponding to a dielectric fluid (FC-77) and heaters manufactured from silicon. With increasing modified Rayleigh number ($10^4 \leq \mathrm{Ra}^*_{L_z} \leq 10^9$), the cavity flow becomes more boundary layer-like along the vertical walls, and multiple fluid cells develop in the central region. Thermal spreading in the substrate increases with decreasing modified Rayleigh number and with increasing values of the substrate/fluid thermal conductivity ratio ($10^{-1} \leq R_s \leq 10^3$). For large R_s, the discrete heat sources lose their thermal identity, and the streamlines and isotherms resemble those associated with a differentially heated cavity. Thermal spreading in the substrate also has a significant effect on circulation in the cavity and on maximum surface temperatures.

Keywords: natural convection; conjugate heat transfer; electronic cooling; numerical simulation

Introduction

As the computer industry moves from large, main-frame systems with multiple terminals to systems of networked, yet independent, work stations and desktop computers, each with its own powerful CPU, alternative cooling technologies will be required. Current work stations and desktop computers typically use forced-air cooling to remove heat from the computer chip surface. With increasing heat removal requirements at the chip level, larger and more powerful fans will be necessary for air cooling, exacerbating problems associated with noise and vibration control. To alleviate these problems, natural convection provides a viable cooling alternative for these powerful, yet portable, computing systems. A major disadvantage to natural convection is that heat transfer rates are small compared to forced convection or boiling. Nevertheless, it may be possible to accommodate higher-power dissipation levels by using a natural convection cooling scheme with the computer chips immersed in a dielectric liquid (Bar-Cohen 1993).

Because relatively low convective heat transfer coefficients are associated with natural convection from small heat sources mounted in a substrate, conduction through the substrate may also influence the heat transfer process. The coupling between conduction in the substrate and convection in the fluid allows for thermal spreading to occur through the substrate and provides an additional heat transfer path from the heat source to the fluid. These conditions are not well defined in most applications, and these interactions are typically ignored with idealized thermal conditions often prescribed at the solid/fluid interface. Sathe and Joshi (1991) have concluded that the simplistic boundary conditions typically prescribed at solid/fluid interfaces are inappropriate for many situations, and a conjugate analysis should be performed.

One of the first investigators to study conjugate effects in natural convection was Zinnes (1970). He concluded that the degree of coupling between conduction in a substrate and natural convection in a fluid is greatly influenced by the substrate/fluid thermal conductivity ratio R_s. Kim and Viskanta (1984) studied the effect of wall conductance on natural convection within a two-dimensional (2-D) cavity. In this study, all of the walls were conductive. They determined that under certain conditions, the local Nusselt number may be inappropriate to describe heat transfer, because it could change sign due to a change in direction of the local heat flux. This behavior was also observed by Du and Bilgen (1992), who numerically investigated the effect of wall conduction on natural convection in a rectangular cavity with only one conductive wall. Joshi and co-workers (Sathe and Joshi 1991, 1992; Joshi et al. 1993; Wroblewski and Joshi, 1992, 1993, 1994) have performed various numerical studies involving conjugate natural convection, and their studies are summarized in the companion paper (Heindel et al. 1995).

Address reprint requests to the T. J. Heindel, Institute of Paper Science and Technology, 500 10th Street NW, Atlanta, GA 30318-5794, USA.

Received 10 March 1995; accepted 10 July 1995

Int. J. Heat and Fluid Flow 16: 511–518, 1995

655 Avenue of the Americas, New York, NY 10010

0142-727X/95/$10.00
SSDI 0142-727X(95)00057-W

This paper numerically investigates the coupled conduction and natural convection transport from an array of discrete heat sources flush mounted to one vertical wall of a cavity. The opposite vertical wall and the horizontal walls are assumed to be isothermal and adiabatic, respectively. Thermal conditions at the heater/fluid and substrate/fluid interfaces are not known a priori but are determined through the solution process. The fluid Prandtl number and heater/fluid thermal conductivity ratio were fixed at 25 and 2350, respectively, corresponding to a dielectric liquid (FC-77) and heaters manufactured from silicon. The modified Rayleigh number, based on application of an isoflux condition to the back of each heater of length L_z, and the substrate/fluid thermal conductivity ratios were varied between $10^4 \leq \mathrm{Ra}^*_{L_z} \leq 10^9$ and $10^{-1} \leq R_s \leq 10^3$, respectively, to determine their effect on conduction within the substrate and convection within the fluid. In the companion paper (Heindel et al. 1995), it was shown that by neglecting edge effects and thermal spreading in the spanwise direction, a 2-D model overpredicts the surface temperatures of the discrete heat sources. However, predictions based on the 2-D model are consistent with experimental trends and require much less computational effort. These may, therefore, be used to determine physical trends associated with an extended parametric range.

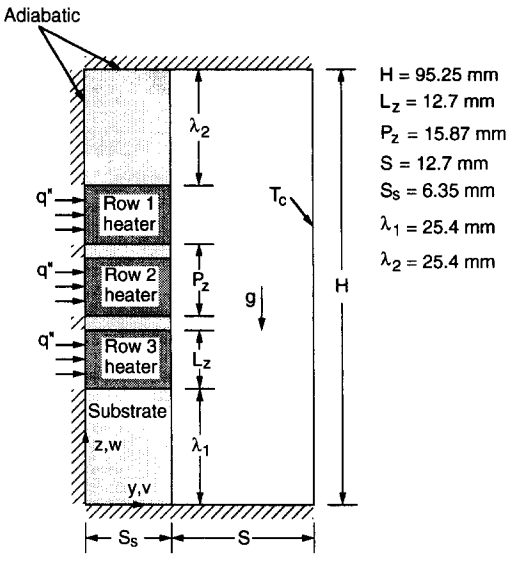

Figure 1 Schematic of the discretely heated cavity

Governing equations

Figure 1 displays a schematic of the geometry used in this investigation, which provides a 2-D approximation of the geometry used in the companion paper (Heindel et al. 1995). One vertical wall is composed of three discrete heat sources flush mounted in a substrate of different thermal conductivity. An isoflux condition is imposed at the back of each heat source, while the back of the substrate is assumed to be adiabatic. An isothermal condition is maintained at the opposing vertical wall, and the horizontal walls are assumed to be adiabatic.

The heater, substrate, and fluid are assumed to have constant but different thermophysical properties. Assuming 2-D steady-state heat transfer, negligible contact resistance between the heater/substrate interface, laminar natural convection with no viscous dissipation, and the Boussinesq approximation, the dimensionless governing equations for the fluid and solid regions can be written as follows:

Fluid:

Continuity:

$$\frac{\partial V}{\partial Y} + \frac{\partial W}{\partial Z} = 0 \tag{1}$$

Y-momentum:

$$V\frac{\partial V}{\partial Y} + W\frac{\partial V}{\partial Z} = \mathrm{Pr}\left(\frac{\partial^2 V}{\partial Y^2} + \frac{\partial^2 V}{\partial Z^2}\right) - \frac{\partial P}{\partial Y} \tag{2}$$

Z-momentum:

$$V\frac{\partial W}{\partial Y} + W\frac{\partial W}{\partial Z} = \mathrm{Pr}\left(\frac{\partial^2 W}{\partial Y^2} + \frac{\partial^2 W}{\partial Z^2}\right) - \frac{\partial P}{\partial Z} + \mathrm{Ra}^*_{L_z}\,\mathrm{Pr}\,\theta \tag{3}$$

Notation

A_z	fluid cavity aspect ratio, H/S
g	acceleration due to gravity
H	cavity height
k_f	fluid thermal conductivity
k_h	heater thermal conductivity
k_s	substrate thermal conductivity
L_z	vertical heater length
P	dimensionless pressure, $\mathrm{p}/\rho(\alpha_f/L_z)^2$
Pr	Prandtl number
P_z	heater pitch
p	pressure
$\hat{q}''$	dimensionless heat flux parameter, $q''\mid_i/q''$
q''	local heat flux applied to the heater back surface of the heat source
$q''\mid_i$	local heat flux at the solid/fluid interface
$\mathrm{Ra}^*_{L_z}$	modified Rayleigh number, $g\beta q'' L_z^4/(k_f \alpha_f \nu)$
R_h	heater/fluid thermal conductivity ratio, k_h/k_f
R_s	substrate/fluid thermal conductivity ratio, k_s/k_f
S	width of cavity fluid region
S_s	width of cavity substrate region
T	local temperature
T_c	cold plate temperature
U_o	reference velocity
V, W	dimensionless velocities, vL_z/α_f and wL_z/α_f
v, w	velocity
Y, Z	dimensionless coordinates, y/L_z and z/L_z
y, z	coordinate directions

Greek

α_f	fluid thermal diffusivity
β	volumetric thermal expansion coefficient
Γ	solid region diffusion coefficient
θ	dimensionless temperature, $(T - T_c)/(q''L_z/k_f)$
λ_1, λ_2	heat source spacings from cavity top and bottom surfaces
ν	kinematic viscosity
ρ	fluid density
Ψ	dimensionless stream function

Energy:

$$V\frac{\partial\theta}{\partial Y}+W\frac{\partial\theta}{\partial Z}=\frac{\partial^2\theta}{\partial Y^2}+\frac{\partial^2\theta}{\partial Z^2} \tag{4}$$

Solid:

Energy:

$$0=\Gamma\left(\frac{\partial^2\theta}{\partial Y^2}+\frac{\partial^2\theta}{\partial Z^2}\right) \tag{5}$$

where

$$Y=\frac{y}{L_z} \qquad Z=\frac{z}{L_z} \tag{6}$$

$$V=\frac{vL_z}{\alpha_f} \qquad W=\frac{wL_z}{\alpha_f} \tag{7}$$

$$P=\frac{p}{\rho(\alpha_f/L_z)^2} \qquad \theta=\frac{T-T_c}{(q''L_z/k_f)} \tag{8}$$

$$\mathrm{Pr}=\frac{\nu}{\alpha_f} \qquad \mathrm{Ra}^*_{L_z}=\frac{g\beta q''L_z^4}{k_f\alpha_f\nu} \tag{9}$$

$$R_s=\frac{k_s}{k_f} \qquad R_h=\frac{k_h}{k_f} \qquad \Gamma=\begin{cases}R_h & \text{in the heater}\\ R_s & \text{in the substrate}\end{cases} \tag{10}$$

The boundary conditions to the above equations are as follows:

$$Y=0: \qquad V=W=0 \qquad \frac{\partial\theta}{\partial Y}=\begin{cases}\dfrac{-1}{R_h} & \text{at the heater}\\ 0 & \text{at the substrate}\end{cases} \tag{11}$$

$$Y=(S_s+S)/L_z: \qquad V=W=0 \qquad \theta=0 \tag{12}$$

$$Z=0: \qquad V=W=0 \qquad \frac{\partial\theta}{\partial Z}=0 \tag{13}$$

$$Z=H/L_z: \qquad V=W=0 \qquad \frac{\partial\theta}{\partial Z}=0 \tag{14}$$

The matching of heat fluxes and temperatures at interfaces of dissimilar materials is implicitly effected through the harmonic mean formulation of the interface conductivities (Patankar 1980).

Solution procedure

The solution procedure used in this study is identical to that described in the companion paper (Heindel et al. 1995) and is only summarized here. The governing partial differential equations were discretized on a nonuniform 40×80 grid using a control–volume formulation and employing the SIMPLER algorithm for the velocity–pressure coupling (Patankar 1980). The iterative solution technique was enhanced by an additive correction multigrid method to speed convergence (Heindel 1994). It is noted that although separate equations are written for the fluid and solid regions, numerical solutions are obtained in both regions simultaneously by solving the continuity, momentum, and energy equations in the entire computational domain. By specifying the correct thermophysical properties in each region, the governing equations are reduced to the appropriate forms for each region.

The overall solution procedure for a particular modified Rayleigh number involved using a previously generated solution at a lower Rayleigh number as input to calculations. The original solutions at $\mathrm{Ra}^*_{L_z}=10^4$ were obtained by specifying very small values (on the order of 10^{-10}) for the initial velocity and temperature distribution. Under-relaxation techniques were used only in the momentum equations, with under-relaxation values decreasing as the modified Rayleigh number increased. The same convergence criteria used in the companion paper were enforced here, and the numerical code was validated against benchmark results for natural convection in a differentially heated cavity (de Vahl Davis 1983).

Results

A parametric study involving 2-D conjugate heat transfer from an array of flush-mounted heat sources was conducted to determine the effects of modified Rayleigh number and substrate/fluid thermal conductivity ratio R_s. The fluid Prandtl number was fixed at 25, which corresponds to FC-77. Previous investigators (Keyhani et al. 1988; Prasad et al. 1990; Sathe and Joshi 1991, 1992) have shown Prandtl number effects to be negligible for $5\le\mathrm{Pr}\le1000$, implying applicability of the results of this study to any fluid whose Prandtl number falls within this range. The prescribed heater thermal conductivity corresponded to that of silicon ($k_h=148$ W/mK), producing a constant heater/fluid thermal conductivity ratio of $R_h=2350$. The cavity geometry (Figure 1) was also fixed, with an aspect ratio of $A_z=H/S=7.5$.

Calculations were performed for modified Rayleigh numbers, based on the applied isoflux condition, and substrate/fluid thermal conductivity ratios in the ranges $10^4\le\mathrm{Ra}^*_{L_z}\le10^9$ and $10^{-1}\le R_s\le10^3$, respectively. These ranges of parameters are believed to encompass values that might be obtained in a practical electronic package. A substrate/fluid thermal conductivity ratio of $R_s=575$ corresponds to an alumina ceramic substrate and FC-77, which is a representative combination for liquid immersion cooling of electronic packages. Also, $\mathrm{Ra}^*_{L_z}=10^9$ corresponds to a 1.27×1.27 cm heat source dissipating 0.35 W/cm^2 with FC-77 as the coolant. The effect of modified Rayleigh number or substrate/fluid thermal conductivity ratio is addressed by fixing all other parameters near the middle of their range of variation. Hence, the effect of modified Rayleigh number is considered for $R_s=10^1$, and the effect of substrate/fluid thermal conductivity ratio is examined for $\mathrm{Ra}^*_{L_z}=10^6$.

Modified Rayleigh number effects

The modified Rayleigh number is varied by altering the total power applied to each heat source, and the effect on the flow field is shown in the streamlines of Figure 2, where the dimensionless stream function is defined by the following:

$$V=\frac{\partial\Psi}{\partial Z} \qquad W=-\frac{\partial\Psi}{\partial Y} \tag{15}$$

The heaters and substrate are also shown for clarity. At $\mathrm{Ra}^*_{L_z}=10^4$ (Figure 2a), the flow is unicellular and weak, with $|\Psi|_{\max}=8.2$. A thick boundary layer envelops a small core of nearly stagnant fluid, which is located slightly above the center of the enclosure. With increasing $\mathrm{Ra}^*_{L_z}$, the boundary layer thins, and the core region enlarges, with additional recirculation zones developing, as small portions of fluid descending along the cold wall are swept toward the leading edges of each heater row. These trends are shown in Figure 2b for $\mathrm{Ra}^*_{L_z}=10^9$, with $|\Psi|_{\max}=192.8$. The flow pattern becomes very complex, with multiple cells developing in the central region of the cavity. Boundary layers along the hot and cold walls, as well as at the cavity ceiling, have thinned considerably and are characterized by large velocities.

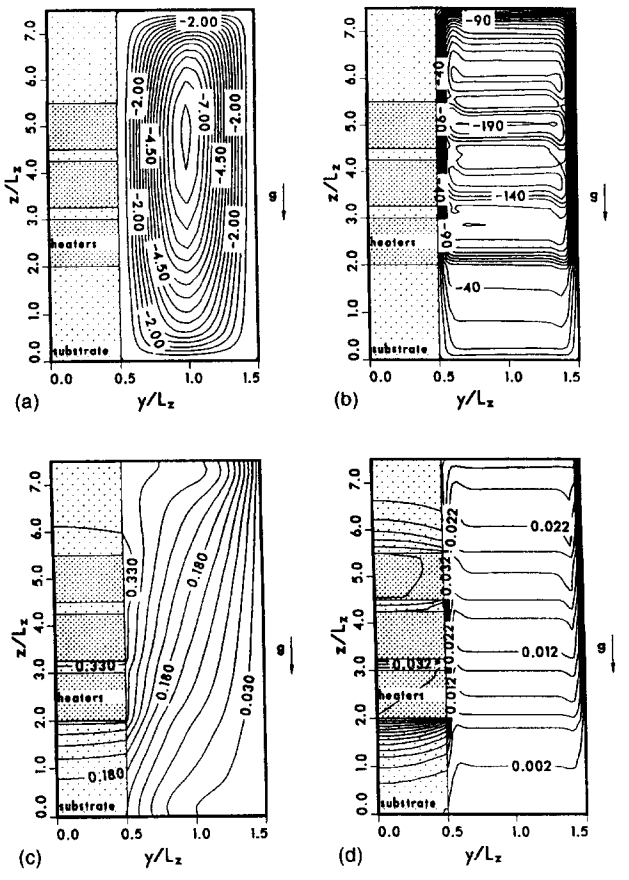

Figure 2 Dimensionless streamlines Ψ at (a) $Ra^*_{L_z} = 10^4$ ($\Delta\Psi = 0.50$); (b) $Ra^*_{L_z} = 10^9$ ($\Delta\Psi = 10.0$); and isotherms θ at (c) $Ra^*_{L_z} = 10^4$ ($\Delta\theta = 0.030$); (d) $Ra^*_{L_z} = 10^9$ ($\Delta\theta = 0.002$) for Pr = 25, $R_h = 2350$, and $R_s = 10^1$

This condition is manifested by the closely spaced streamlines, which appear as thick bands at several locations. Some of the fluid descending the cold wall is swept toward the hot wall near the leading edge of each heater row, with the majority of the transfer occurring near the leading edge of row three. Some fluid also descends to the bottom of the cavity, but relative to other regions, this flow is weak.

Figure 2c shows the nondimensional isotherms θ in both the fluid and solid regions for $Ra^*_{L_z} = 10^4$, where, as indicated by the almost vertical isotherms, heat transfer through the fluid region is dominated by conduction. With increasing $Ra^*_{L_z}$ however, the core region begins to thermally stratify, and at $Ra^*_{L_z} = 10^9$ (Figure 2d), the central region of the fluid is completely stratified, and the hot and cold wall thermal boundary layers are extremely thin. Each heater face is isothermal because of its large thermal conductivity, although temperatures do differ from one heater to another. The dimensionless temperature θ decreases with increasing $Ra^*_{L_z}$, because the increase in $(T - T_c)$ is not commensurate with the corresponding increase in q''.

A dimensionless local heat flux at the solid/fluid interface is defined as

$$\hat{q}'' = \frac{q''|_i}{q''} \tag{16}$$

where $q''|_i$ is the local heat flux at the solid/fluid interface. The variation in $\hat{q}''$ with location along the interface is shown in Figure 3 for the full range of modified Rayleigh numbers and $R_s = 10^1$. In all cases, a local spike exists at the leading edge of each heater row, because of the large value of the local convection coefficient. The largest value of $\hat{q}''$ occurs at the leading edge of row three ($z/L_z = 2.0$), with successively smaller values characterizing the leading edges of rows two and one. On each heater, $\hat{q}''$ increases with increasing $Ra^*_{L_z}$ caused by thinning of the thermal boundary layer and, hence, an increase in the local convection coefficient. However, because of reduced thermal spreading with increasing $Ra^*_{L_z}$, the opposite behavior characterizes conditions at the substrate/fluid interface. That is, $\hat{q}''$ decreases with increasing $Ra^*_{L_z}$ in this region.

For smaller values of $Ra^*_{L_z}$, a second, smaller, peak in $\hat{q}''$ exists at the trailing edge of the downstream heaters. This peak is most apparent at the trailing edge of row one ($z/L_z = 5.5$) and is attributed to significant streamwise conduction (relative to advection) in the fluid. Streamwise conduction is, of course, also present at the leading edge of each heater, but its presence is masked by the high local convection coefficient caused by the inception of heating. As advection increases with increasing $Ra^*_{L_z}$, local enhancement caused by streamwise conduction diminishes and eventually is completely suppressed.

The local nondimensional temperature along the solid/fluid interface (θ_{sur}) is displayed in Figure 4. The solid/fluid interface temperature continuously increases from the cavity bottom ($z/L_z = 0$) to the leading edge of row three ($z/L_z = 2.0$). The isothermal heater faces for each row are clearly displayed. Because of the thickening thermal boundary layer, θ_{sur} increases from row three to row one. The substrate regions between heater rows also show a general increase in θ_{sur} with Z/L_z. However, θ_{sur} may initially diminish slightly because of partial dissipation of the thermal boundary layer when advection is strong. At the trailing edge of row one ($z/L_z = 5.5$), the thermal boundary layer dis-

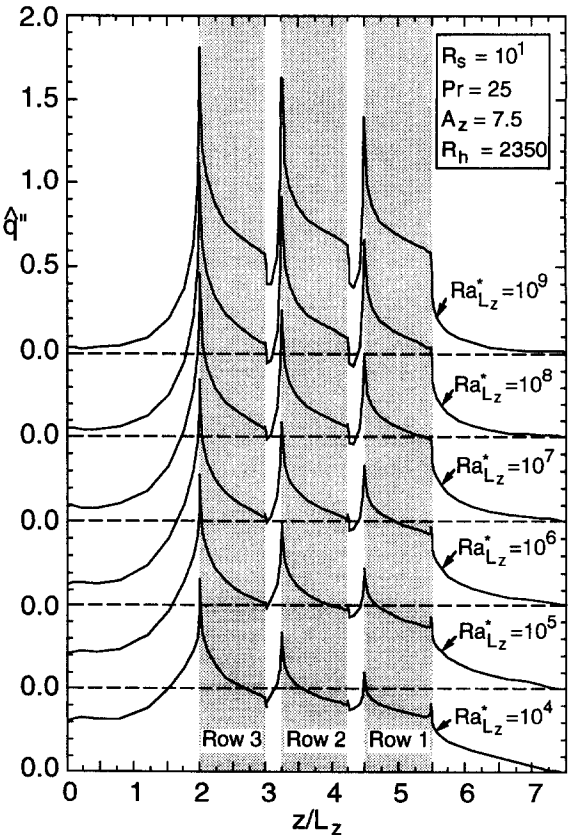

Figure 3 Effect of modified Rayleigh number on the local dimensionless heat flux for Pr = 25, $R_h = 2350$, and $R_s = 10^1$

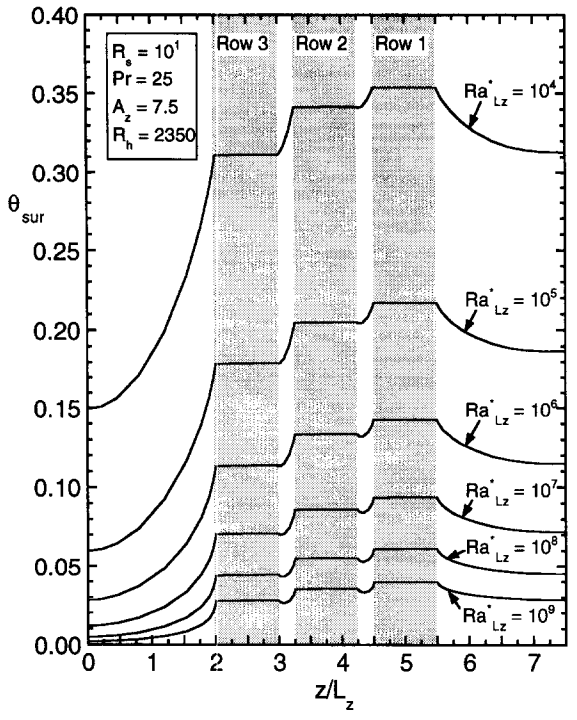

Figure 4 Effect of modified Rayleigh number on the local dimensionless temperature profiles at the solid/fluid interface for Pr = 25, $R_h = 2350$, and $R_s = 10^1$

perses, and θ_{sur} decreases monotonically with Z beyond that location. The decrease in the nondimensional temperature with increasing $Ra^*_{L_z}$ is also demonstrated.

Effect of substrate/fluid thermal conductivity ratio

The effect of the substrate/fluid thermal conductivity ratio on fluid flow and heat transfer within a discretely heated cavity is examined by fixing the modified Rayleigh number at $Ra^*_{L_z} = 10^6$. Dimensionless streamlines Ψ and isotherms θ for two different substrate/fluid thermal conductivity ratios are presented in Figure 5. At $R_s = 10^{-1}$, flow below row three is virtually nonexistent (Figure 5a), with a stagnant core region located close to the top of the cavity and $|\Psi|_{max} = 47.0$. Cool fluid traverses central regions of the cavity from the cold wall to the hot wall at vertical locations corresponding roughly to the leading edge of each heater row, with most of the fluid traversing the cavity near the leading edge of row three. Increasing the thermal conductivity ratio yields a region of fluid flow below row three, causing the core to descend toward the center of the cavity. When $R_s = 10^3$ (Figure 5b), $|\Psi|_{max}$ increases to 53.5, and the resulting flow pattern is typical of that associated with a cavity having isothermal hot and cold walls (Yang 1987). The stagnant core is located in the center of the fluid region, and most of the fluid traverses the entire cavity. Flow regions associated with the discrete heat sources also become indistinguishable when the substrate and heater thermal conductivities are of the same order, as long as R_s and R_h are both much greater than unity.

Isotherms for the foregoing conditions are also shown in Figure 5. With $R_s = 10^{-1}$ (Figure 5c), conduction through the substrate is substantially suppressed, and the lower region of the cavity, extending from the hot to the cold wall, is almost isothermal. Because of the large thermal conductivity of the heaters, each heater face is also nearly isothermal. However, the low thermal conductivity of the substrate yields significant differences between the heater temperatures. Because of larger adjoining thermal boundary thicknesses and higher local fluid temperatures, heater temperatures increase from row three to row one.

Substrate conduction increases with increasing R_s, and the lower fluid region is no longer isothermal across the entire cavity width. Maximum dimensionless temperatures decrease with increasing R_s, as more thermal spreading occurs throughout the substrate before energy is convected to the fluid. At the highest substrate/fluid thermal conductivity ratio of $R_s = 10^3$ (Figure 5d), the fluid isotherms are almost diagonally symmetric, resembling those associated with a differentially heated cavity (Yang 1987). Because the substrate and heater thermal conductivities are comparable and their depth S_s is sufficient for significant thermal spreading, the substrate and heaters are at a nearly uniform temperature along the solid/fluid interface.

The spatial variation in the dimensionless heat flux is shown in Figure 6 for $Ra^*_{L_z} = 10^6$ and different values of R_s. At $R_s = 10^{-1}$, the substrate acts as a good insulator, and little energy is transported through the substrate to the fluid. The discrete heat sources are easily distinguished by the spikes associated with initiation (or reinitiation) of the thermal boundary layer at the leading edge of each heater. The spikes in $\hat{q}''$ at the trailing edge of each heater for $R_s = 10^{-1}$ are due to the enhancement caused by streamwise diffusion in this region. The amount of energy entering the fluid through the heater face decreases with increasing R_s, while the opposite trend exists at the substrate/fluid interface. The magnitudes of the leading and trailing edge spikes also decrease with increasing R_s. At $R_s = 10^1$, the discrete heat sources begin to lose their thermal identity,

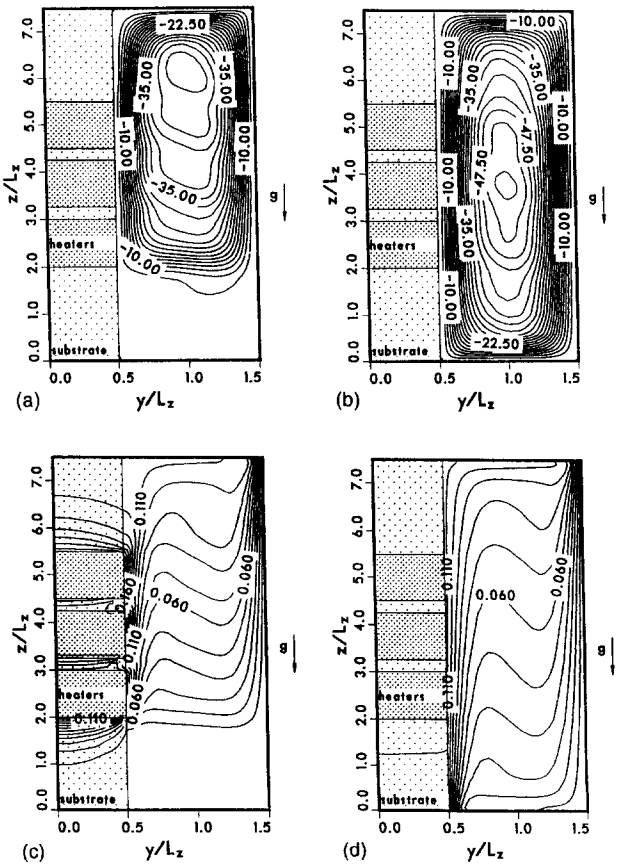

Figure 5 Dimensionless streamlines Ψ at (a) $R_s = 10^{-1}$ ($\Delta\Psi = 2.50$); (b) $R_s = 10^3$ ($\Delta\Psi = 2.50$); and isotherms θ at (c) $R_s = 10^{-1}$ ($\Delta\theta = 0.010$); (d) $R_s = 10^3$ ($\Delta\theta = 0.010$) for Pr = 25, $R_h = 2350$, and $Ra^*_{L_z} = 10^6$

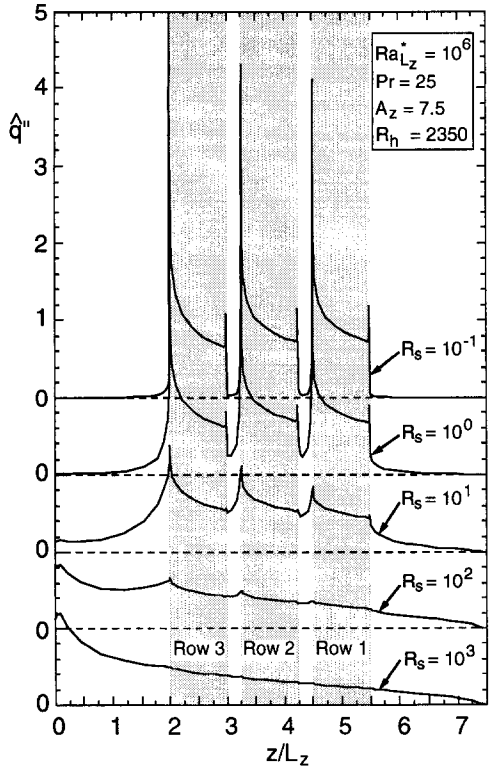

Figure 6 Effect of substrate thermal conductivity on the local dimensionless heat flux for Pr = 25, $R_h = 2350$, and $Ra^*_{L_z} = 10^6$

and they become difficult to locate at $R_s = 10^2$. For $R_s = 10^3$, the distribution of $\hat{q}''$ more closely resembles that associated with a differentially heated cavity. This result has important implications in electronics cooling, where a realistic value of R_s for an alumina substrate and dielectric liquid coolant would be approximately 575.

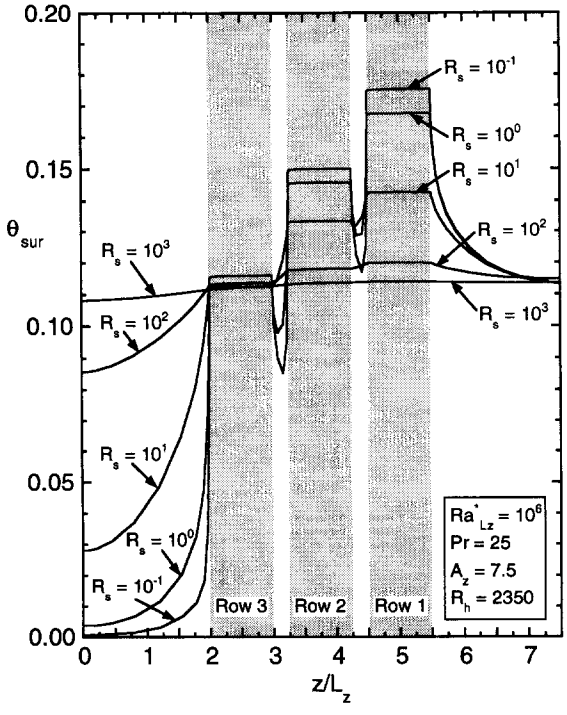

Figure 7 Effect of substrate thermal conductivity on the local dimensionless temperature distribution along at the solid/fluid interface for Pr = 25, $R_h = 2350$, and $Ra^*_{L_z} = 10^6$

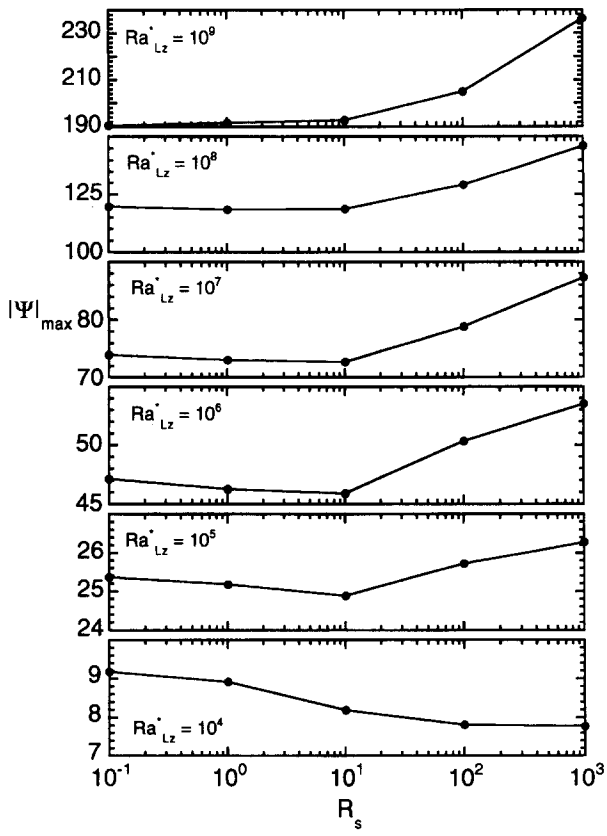

Figure 8 Maximum $|\Psi|$ for Pr = 25 and $R_h = 2350$

Temperature variations at the solid/fluid interface for all R_s values are shown in Figure 7. At $R_s = 10^{-1}$, thermal spreading is weak, and large θ_{sur} variations are observed between substrate and heater regions, as well as from heater row-to-heater row. Increasing R_s allows for more thermal spreading through the substrate, reducing the temperature variations at the solid/fluid interface, with the interface becoming nearly isothermal over the entire cavity height when $R_s = 10^3$.

Conjugate interactions

The maximum temperature increase experienced by a fluid element, $\Delta T_{max} = (T - T_c)_{max}$, is related to the buoyant potential. A larger temperature difference signifies a larger buoyant potential and stronger fluid circulation. In this conjugate analysis, ΔT_{max} increases with increasing $Ra^*_{L_z}$ but decreases with increasing R_s for a fixed modified Rayleigh number. Hence, a reduction in ΔT_{max} with increasing R_s implies a reduction in the buoyant driving potential and a decline in the cavity circulation. Increasing R_s also increases conduction through the substrate and allows energy to enter the fluid below row three, thereby preheating the fluid in this region and inducing fluid motion. The corresponding increase in fluid momentum offsets, to some extent, the effect of the reduced buoyancy potential. Consequently, the net effect on the cavity circulation of increasing R_s is determined by a reduction in the buoyancy potential, as well as by increased acceleration of the fluid caused by heat transfer from the substrate.

A measure of the flow intensity (cavity circulation) is provided by the absolute value of the maximum stream function, $|\Psi|_{max}$. As shown in Figure 8, this quantity depends on the

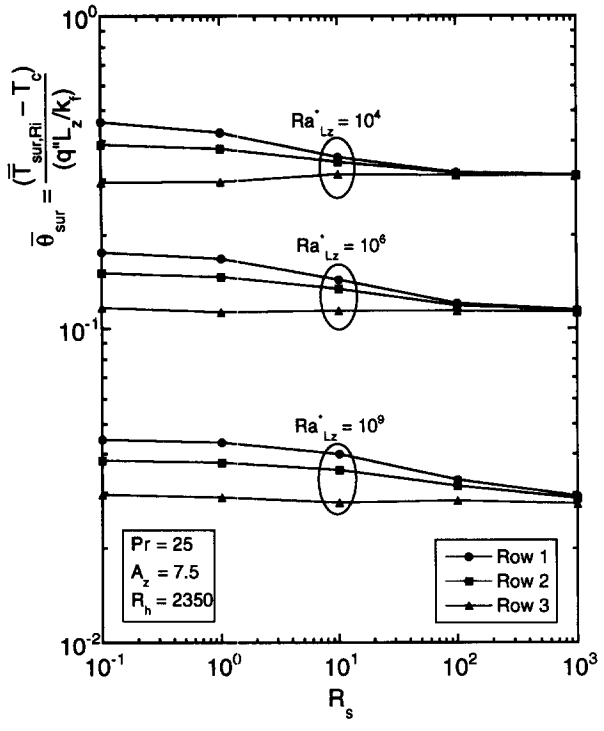

Figure 9 Average dimensionless heater surface temperature for Pr = 25, $R_h = 2350$, and $Ra^*_{L_z} = 10^4$, 10^6, and 10^9

substrate/fluid thermal conductivity ratio, as well as the modified Rayleigh number. For a fixed value of R_s, $|\Psi|_{max}$ increases monotonically with increasing $Ra^*_{L_z}$. However, for a fixed modified Rayleigh number, $|\Psi|_{max}$ may increase or decrease with increasing R_s.

At $Ra^*_{L_z} = 10^4$, the flow intensity decreases with increasing R_s. For this modified Rayleigh number, there is very slow fluid motion, and heat transfer is conduction dominated. With increasing R_s, heat transfer to the fluid becomes less localized, and fluid motion is induced in a larger portion of the cavity. The associated increase in viscous drag results in a reduction in flow intensity. For $10^5 \le Ra^*_{L_z} \le 10^7$, there is a local minimum in flow intensity at $R_s = 10^1$. For $10^{-1} \le R_s \le 10^1$, increasing R_s produces just a few streamlines that penetrate the lower region of the cavity. The change in flow structure is not significant enough to overcome the influence of the reduction in buoyancy potential, resulting in an overall decrease in flow intensity. In contrast, for $10^1 < R_s \le 10^3$, the discrete heat sources lose much of their thermal identity, and the flow acquires the simple structure shown in Figure 5b. In this case, sustained fluid acceleration caused by substrate heating more than compensates for the smaller buoyancy potential. At $Ra^*_{L_z} \ge 10^8$, the effect of the reduced buoyancy potential is closely balanced by changes in flow structure when $R_s \le 10^1$, and very little change in $|\Psi|_{max}$ is observed. However, once the discrete heat sources begin to lose their thermal identity ($R_s > 10^1$), a significant increase in the flow intensity is observed.

The effect of R_s on the average dimensionless surface temperature of each heater is shown in Figure 9. The actual average surface temperature increases with increasing $Ra^*_{L_z}$, because more energy is being transferred to the cavity. However, the average dimensionless surface temperature decreases because of the definition of θ (Equation 8). For small values of R_s, the average heater temperature increases from row three to row one, because the thermal boundary-layer thickness increases along the heated wall, and thermal spreading is minimal. As R_s approaches R_h, thermal spreading occurs throughout the substrate, yielding greater temperature uniformity among the heaters and reducing the maximum heater temperature.

Conclusions

In a rectangular cavity with flush-mounted discrete heat sources, heat transfer is dominated by conduction at small values of the modified Rayleigh number ($Ra^*_{L_z} \approx 10^4$). With increasing $Ra^*_{L_z}$, flow becomes more boundary layer-like along the vertical walls, with multiple fluid cells developing in the central fluid (core) region. The core region also becomes more thermally stratified, and the amount of substrate conduction decreases. As the substrate/fluid thermal conductivity ratio increases, fluid flow is induced below the heater array, and the core region moves downward from near the cavity ceiling for $R_s = 10^{-1}$ toward the cavity center for $R_s = 10^3$. At $R_s = 10^1$, the discrete heat sources begin to lose their thermal identity, and when $R_s \approx 10^3$, the discrete heater locations become almost indistinguishable. For $R_s \approx 10^3$, streamlines and isotherms resemble those associated with a differentially heated cavity.

The intensity of fluid motion is influenced in various ways by the substrate/fluid thermal conductivity ratio. At $Ra^*_{L_z} = 10^4$, the intensity decreases with increasing R_s; whereas, the opposite trend exists when $Ra^*_{L_z} \ge 10^8$. For $10^5 \le Ra^*_{L_z} \le 10^7$, a local minimum in flow intensity exists at $R_s = 10^1$. Increasing the substrate/fluid thermal conductivity ratio enhances thermal spreading, thereby reducing differences between average surface temperatures of the three heaters, as well as the maximum heater surface temperature.

Acknowledgments

Support of this work by the National Science Foundation under Grant No. CTS-9004213 is gratefully acknowledged.

References

Bar-Cohen, A. 1993. Physical design of electronic systems—Methodology, technical trends, and future challenges. In *Advances in Thermal Modeling of Electronic Components and Systems*, Vol. 3, A. Bar-Cohen and A. D. Kraus (eds.), ASME/IEEE Press, New York, 1–60

de Vahl Davis, G. 1983. Natural convection of air in a square cavity: A benchmark numerical solution. *Int. J. Num. Meth. Fluids*, **3**, 249–264

Du, Z.-G. and Bilgen, E. 1992. Coupling of wall conduction with natural convection in a rectangular enclosure. *Int. J. Heat Mass Transfer*, **35**, 1969–1975

Heindel, T. J. 1994. A numerical and experimental study of three-dimensional natural convection in a discretely heated cavity. Ph.D. thesis, Purdue University, West Lafayette, IN

Heindel, T. J., Ramadhyani, S. and Incropera, F. P. 1995. Conjugate natural convection from an array of discrete heat sources: Part 1—Two- and three-dimensional model validation. *Int. J. Heat Fluid Flow*, **16**, 501–510

Joshi, Y., Haukenes, L. O. and Sathe, S. B. 1993. Natural convection liquid immersion cooling of a heat source flush mounted on a conducting substrate in a square enclosure. *Int. J. Heat Mass Transfer*, **36**, 249–263

Keyhani, M., Prasad, V., Shen, R. and Wong, T.-T. 1988. Free convection heat transfer from discrete heat sources in a vertical cavity. *Natural and Mixed Convection in Electronic Equipment Cooling*, ASME HTD-Vol. 100, R.A. Wirtz (ed.), ASME Press, New York, 13–29

Kim, D. M. and Viskanta, R. 1984. Study of the effects of wall conductance on natural convection in differently oriented square cavities. *J. Fluid Mech.*, **144**, 153–176

Patankar, S. V. 1980. *Numerical Heat Transfer and Fluid Flow*. Hemisphere Publishing, Bristol, PA

Prasad, V., Keyhani, M. and Shen, R. 1990. Free convection in a discretely heated vertical enclosure: Effects of Prandtl number and cavity size. *J. Electronic Packaging*, **112**, 63–74

Sathe, S. B. and Joshi, Y. 1991. Natural convection arising from a heat generating substrate-mounted protrusion in a liquid-filled two-dimensional enclosure. *Int. J. Heat Mass Transfer*, **34**, 2149–2163

Sathe, S. B. and Joshi, Y. 1992. Natural convection liquid cooling of a substrate-mounted protrusion in a square enclosure: A parametric study. *J. Heat Transfer*, **114**, 401–409

Wroblewski, D. and Joshi, Y. 1992. Transient natural convection from a leadless chip carrier in a liquid filled enclosure: A numerical study. In *Advances in Electronic Packaging — 1992*, EEP-Vol. 1-1, W. T. Chen and H. Abé (eds.), ASME Press, New York, 235–248

Wroblewski, D. E. and Joshi, Y. 1993. Computations of liquid immersion cooling for a protruding heat source in a cubical enclosure. *Int. J. Heat Mass Transfer*, **36**, 1201–1218

Wroblewski, D. E. and Joshi, Y. 1994. Liquid immersion cooling of a substrate-mounted protrusion in a three-dimensional enclosure: The effects of geometry and boundary conditions. *J. Heat Transfer*, **116**, 112–119

Yang, K. T. 1987. Natural convection in enclosures. In *Handbook of Single-Phase Heat Transfer*, S. Kakac, R. Shah and W. Aung (eds.), Wiley, New York, 13.1–13.51

Zinnes, A. E. 1970. The coupling of conduction with laminar natural convection from a vertical flat plate with arbitrary surface heating. *J. Heat Transfer*, **92**, 528–535